[Article ID] 1003- 6326(2002)03- 0466- 04

Effects of Zr on crystallization kinetics of Pr-Fe-B amorphous alloys①

LIU Jian-hua(刘建华), LI Wei(李 伟), CHEN Yan(谌 岩), GUAN Ying(关 颖)
(College of Materials and Chemical Engineering, Yanshan University, Qinhuangdao 066004, China)

[Abstract] The effects of Zr on crystallization kinetics of Pr-Fe-B amorphous alloys have been investigated by DTA and XRD methods. It was found that for $Pr_8Fe_{86-x}Zr_xB_6$ (x = 0, 1, 2) amorphous alloys, the final crystallized mixture is α-Fe and $Pr_2Fe_{14}B$, and the metastable $Pr_2Fe_{23}B_3$ phase occurs during crystallization of $Pr_8Fe_{86}B_6$ amorphous alloy, not during crystallization of $Pr_8Fe_{86-x}Zr_xB_6$ (x = 1, 2) amorphous alloys. By analyzing the activation energy of crystallization, the formation of an α-Fe/$Pr_2Fe_{14}B$ composite microstructure with a coarse grain size in annealed $Pr_8Fe_{86}B_6$ alloy, is attributed to a difficult nucleation and an easy growth for both the α-Fe and $Pr_2Fe_{14}B$ in the alloy. The addition of Zr can be used to change the crystallization behavior of the α-Fe phase in Pr-Fe-B amorphous alloy, which is helpful to reduce the grain size for the α-Fe phase.

[Key words] Pr-Fe-B amorphous alloys; Zr; crystallization kinetics; activation energy
[CLC number] TG 139+.8 [Document code] A

1 INTRODUCTION

Nanocomposite magnets consisting of a two-phase distribution of hard-magnetic grains and soft-magnetic grains have attracted considerable interest since they could, by exchange coupling, potentially provide a maximum energy product, $B_{H,max}$, in excess of 796 kJ/m^3[1], which is much larger than any single-phase magnetic material. Unfortunately, the energy product $B_{H,max}$, 79.6 ~ 159.2 kJ/m^3, was much lower than the theoretical value 796 kJ/m^3. Some works[2~10] have shown that the microstructure parameters of practical nanocomposite magnets deviated largely from the calculation predicted by theoretical models for optimum coupling. Especially, the grain size (20 ~ 100 nm) was much larger than the required theoretical calculation (< 10 nm). Recently, Zhang[11] have prepared nanocomposite magnetic alloys with the grain size about 10 nm by the high-pressure technique, the energy product $B_{H,max}$ was 199 kJ/m^3[12]. Hence, it should be a significant way for nanocomposite magnets to increase the maximum energy product by reducing grain size, and controlling the microstructure in magnetic alloys. So the methods, the addition of alloy element and the substitution of element, were introduced. Pr-Fe-B alloy is a new composite permanent magnet on the foundation of Nd-Fe-B alloy. The results showed that the addition of Zr can increase the energy product by reducing the grain size in Pr-Fe-B alloy. However, the effect of Zr during crystallization is short of the theoretical analysis. In this article, a method to prepare nanocomposite magnets is the crystallization of amorphous alloy[13~16]. For the nanocomposite magnets prepared by this method, their microstruture formation is strongly dependent on the crystallization behavior of amorphous alloy. So, the crystallization kinetics of amorphous $Pr_8Fe_{86-x}Zr_xB_6$ (x = 1, 2) alloy will reveal the cause for a coarse grain size and microstructural formation in nanocomposite magnets, and the crystallization effect of Zr in Pr-Fe-B amorphous alloys. These studies will provide a guide to reduce the grain size of nanocomposite magnets and control their microstruture according to theory model, as well as make further improvements for the energy product of the magnets.

2 EXPERIMENTAL

The $Pr_8Fe_{86-x}Zr_xB_6$ (x = 0, 1, 2) alloys were prepared by melting the pure constituent elements with vacuum arc furnace. The ribbons were 20 μm thick and 2 ~ 3 mm wide. The amorphous nature of the ribbons was confirmed by X-ray diffraction (XRD). The structure evolutions and crystallization kinetics of the as-quenched ribbons were investigated by a Perkin-Elmer seven differential thermal analysis (DTA) system and XRD (CuK_α), with a heating rate of 10, 15, and 20 ℃/min, respectively.

The average activation energy of crystallization E_c was calculated by Kissinger method[15]:

$$\mathrm{Ln}(BT^{-2}) = -E_c(RT)^{-1} + \text{constant} \quad (1)$$

The activation energy of crystallization E_x at a certain crystallized fraction x was calculated by Doyle method[15]:

$$\lg B = \lg AE[AF(x)]^{-1} - 2.315 - 0.4567E_x(RT)^{-1} \quad (2)$$

where B is the heating rate, R is the gas constant,

① [Foundation item] Project (19974035) supported by the National Natural Science Foundation of China and project (599240) supported by the Natural Science Foundation of Hebei Province [Received date] 2001- 08- 09; [Accepted date] 2001- 10- 15

T is the temperature, x is the crystallized fraction of crystal, A is the frequency factor, and $F(x)$ is the function which only related to crystallized fraction, x. One could obtain the slope of the plot for $\lg B$ vs T^{-1} and $\lg(BT^{-2})$ vs T^{-1} according to Eqn. (1) and Eqn. (2), by which E_c and E_x are calculated at a given crystallized fraction x for the crystal.

3 RESULTS AND DISCUSSION

3.1 Crystallization of elevating temperature with constant rate

By differential thermal analysis scans, the samples of $Pr_8Fe_{86}B_6$ are found to transform in three steps from amorphous alloy, which are heated to 900 ℃ with heating rate of 10, 15, 20 ℃/min. Hereafter, the X-ray diffraction analysis that the first exothermal peak is for precipitation of the α-Fe phase, the second for metastable $Pr_2Fe_{23}B_3$, and the third for $Pr_2Fe_{14}B$. However, for $Pr_8Fe_{86-x}Zr_xB_6$ (x = 1, 2) alloy, only the exothermal peak of α-Fe phase is distinct. By X-ray diffraction analysis, it is known that the final crystallized phases are α-Fe and $Pr_2Fe_{14}B$ in $Pr_8Fe_{86-x}Zr_xB_6$ (x = 0, 1, 2) alloy, but the metastable $Pr_2Fe_{23}B_3$ disappears with the process of crystallization in $Pr_8Fe_{86-x}Zr_xB_6$ (x = 1, 2) alloy (as is consistent with the result in Ref. [17]). The crystallization temperatures and the DTA results are presented in Table 1 and Fig. 1. Obviously, the addition of Zr changed the crystallization behavior and increased crystallization temperatures of α-Fe phase in Pr-Fe-B alloy.

Fig. 2 shows the curves of crystallized volume fraction (φ_c) of α-Fe phase versus temperature in these three alloys at different heating rates determined by DTA. The largest increase of crystallization rate is found in a wide range of the crystallized fraction from 10% to 90%.

3.2 Activation energy of crystallization

The exothermal peak of $Pr_2Fe_{14}B$ is not distinct in DTA curves due to the addition of Zr, so the effect of Zr on the crystallization behavior of α-Fe has been discussed in this article. According to crystallized peaks data in Table 1, linear relation of $\ln(BT^{-2})$

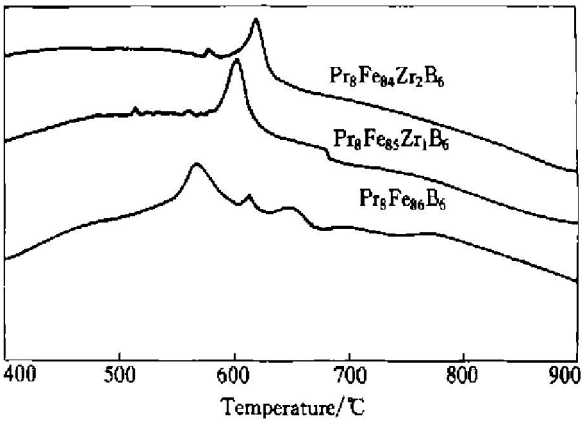

Fig. 1 DTA curves of $Pr_8Fe_{86-x}Zr_xB_6$ (x = 0, 1, 2) amorphous alloy at heating rate of 10 ℃/min

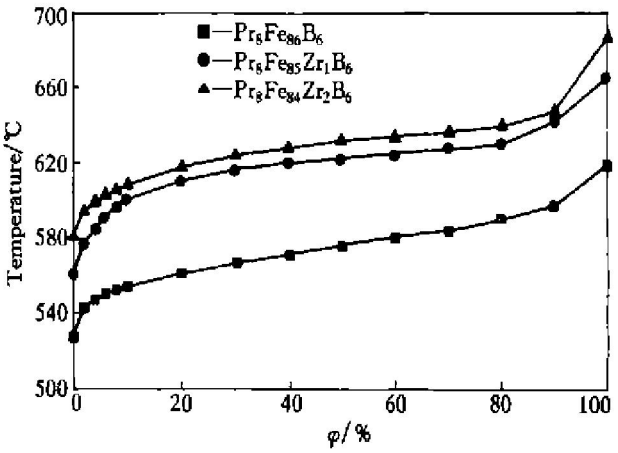

Fig. 2 Dependence of crystallized volume fraction (φ_c) of α-Fe phase on temperature of $Pr_8Fe_{86-x}Zr_xB_6$ (x = 0, 1, 2) amorphous alloys at heating rate of 10 ℃/min

with T^{-1} is obtained, as shown in Fig. 3. By these slope, the average activation energy of α-Fe phase are respectively calculated by Eqn. (1). In the same way, those of $Pr_2Fe_{23}B$ and $Pr_2Fe_{14}B$ phases in $Pr_8Fe_{86}B_6$ alloy are obtained, as shown in Table 2.

Fig. 4 and Fig. 5 show dependence of activation energy of crystallization on their crystallized fraction by Eqn. (2). The activation energy curves in Fig. 4 show that the activation energies of crystallization for α-Fe phase, $Pr_2Fe_{23}B$ and $Pr_2Fe_{14}B$ in amorphous $Pr_8Fe_{86}B_6$ alloy, at the beginning stage of crystalliza-

Table 1 Peak temperature of crystallization of $Pr_8Fe_{86-x}Zr_xB_6$ amorphous alloys at different heating rates (℃)

Heating rates /(℃·min^{-1})	$Pr_8Fe_{86}B_6$			$Pr_8Fe_{85}Zr_1B_6$	$Pr_8Fe_{84}Zr_2B_6$
	α-Fe	$Pr_2Fe_{23}B_3$	$Pr_2Fe_{14}B$	α-Fe	α-Fe
10	575.77	625.19	666.36	625.93	637.08
15	587.20	630.34	671.29	634.38	645.17
20	594.15	635.48	671.81	650.17	658.93

Table 2 Local activation energy of $Pr_8Fe_{86-x}Zr_xB_6$ amorphous alloys (kJ·mol^{-1})

$Pr_8Fe_{86}B_6$			$Pr_8Fe_{85}Zr_1B_6$	$Pr_8Fe_{84}Zr_2B_6$
α-Fe	$Pr_2Fe_{23}B$	$Pr_2Fe_{14}B$	α-Fe	α-Fe
214.88	442.28	661.14	234.54	252.41

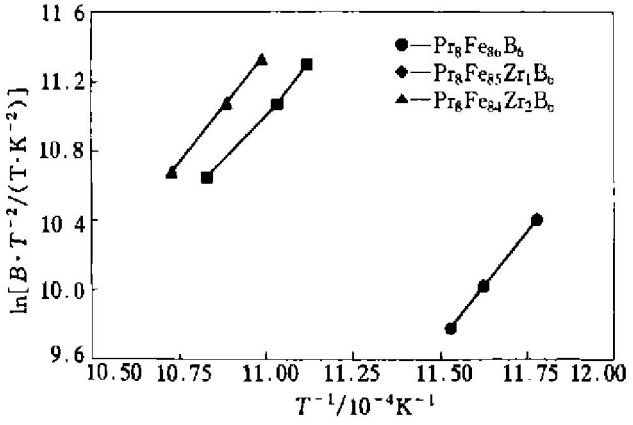

Fig. 3 Plot of $\ln(BT^{-2})$ —T^{-1} at DTA peak temperature of α-Fe phase in $Pr_8Fe_{86-x}Zr_xB_6$ (x = 0, 1, 2) amorphous alloys

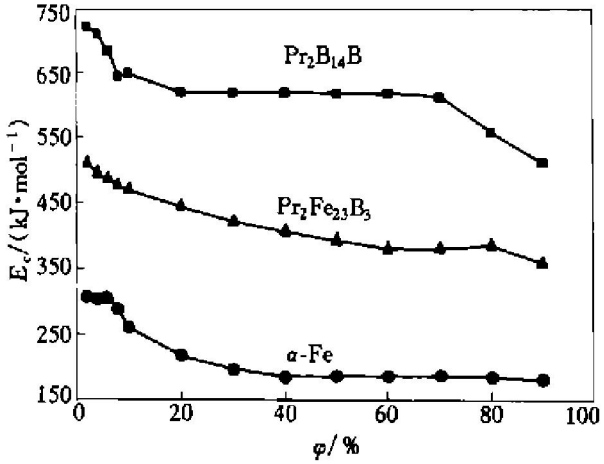

Fig. 4 Dependence of activation energy of crystallization of phases in amorphous $Pr_8Fe_{86}B_6$ alloy on their crystallized fraction

tion are about 306.09, 510.85 and 725.90 kJ/mol, respectively. The activation energy curve of α-Fe phase shows little change as the crystallized fraction is below 8%, then the activation energy decreases with increasing the crystallized fraction. While activation energy of crystallization for $Pr_2Fe_{23}B$ and $Pr_2Fe_{14}B$ decrease with the crystallized fraction. In the crystallization process, activation energies of $Pr_2FE_{23}B$ and $Pr_2Fe_{14}B$ are larger than that of α-Fe phase in the $Pr_8Fe_{86}B_6$ alloy. This indicates that the formation of $Pr_2Fe_{23}B$ and $Pr_2Fe_{14}B$ is more difficult than that of α-Fe phase, which is mainly attributed to the fact that the formation and growth of the $Pr_2Fe_{23}B$ and $Pr_2Fe_{14}B$ depend on not only the diffusion of atoms

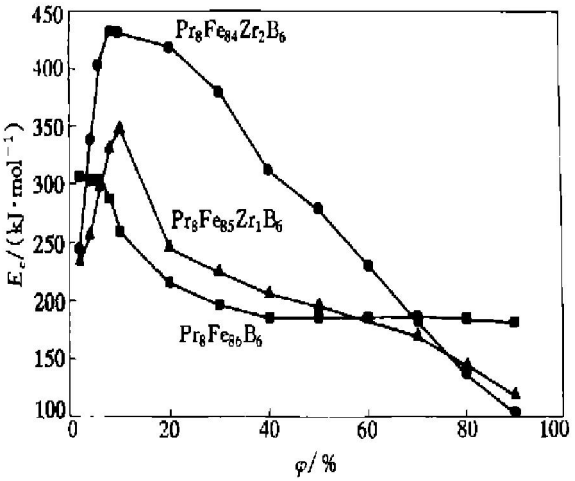

Fig. 5 Dependence of activation energy of crystallization of α-Fe phase in $Pr_8Fe_{86-x}Zr_xB_6$ (x = 0, 1, 2) amorphous alloys on their crystallized fraction

Fe, Pr and B, but also a proper ratio among these atoms for the formation and growth.

To $Pr_8Fe_{86}B_6$ alloy, the larger activation energies of α-Fe and $Pr_2Fe_{14}B$ phase, during the beginning stage of crystallization, show that crystallization and nucleation is difficult for α-Fe and $Pr_2Fe_{14}B$ phase[14, 15]. With the crystallization process, the activation energies of α-Fe and $Pr_2Fe_{14}B$ phase decrease, which means the grains of α-Fe and $Pr_2Fe_{14}B$ phase are easy to grow due to decreasing the crystallization resistance. Obviously, the crystallization behavior of α-Fe phase and $Pr_2Fe_{14}B$ essentially results in the formation of α-Fe phase/$Pr_2Fe_{14}B$ composite structure with a coarse grain size in annealed $Pr_8Fe_{86}B_6$ alloy, which is attributed to a difficult nucleation and easy growth for both α-Fe phase and $Pr_2Fe_{14}B$.

However, as shown in Fig. 5, at the beginning stage of crystallization, there are lower activation energies of α-Fe phase in $Pr_8Fe_{85}Zr_1B_6$ and $Pr_8Fe_{84}Zr_2B_6$, being about 201.18 and 212.68 kJ/mol, respectively. With increasing crystallized fraction, the maximum activation energies obtained at φ= 10% are 57.58 kJ/mol and 142.04 kJ/mol larger than α-Fe phase in $Pr_8Fe_{86}B_6$ alloy, respectively. Furthermore, the activation energy of crystallization of α-Fe phase in $Pr_8Fe_{85}Zr_1B_6$ increases during their crystallization process, which makes the growth of α-Fe phase more difficult than that in $Pr_8Fe_{86}B_6$ alloy. This is helpful to the formation of the α-Fe phase with a fine grain size in amorphous alloy (as is consistent with the result in Ref. [17]).

Additional Zr can change the crystallization behavior of the α-Fe phase in the amorphous Pr-Fe-B alloys, and be helpful to form α-Fe phase with a fine grain size, which is attributed to the effect of Zr on crystallization of Pr-Fe-B amorphous alloy. Zr can be

mainly used to increase electrovalent bond Pr-Zr, Fe-Zr, Zr-B, making electrovalent bond more complicated. Especially, mutual action between Zr and B is largest in electrovalent bond[18]. In addition, due to adding Zr, there are more elements and atom-radius (of which, Pr > Zr > Fe > B) variety, making "chaos" and cumulating density improved. Morover, with the precipitation of α-Fe, a great deal atoms Pr, B, Zr are pushed out into amorphous region, and some atoms Zr, B can enrich around boundary of α-Fe, forming much steady clusters, which can strongly restrain diffusing of atom Fe and boundary moving of α-Fe. It is the reason why grain of α-Fe is difficult to growing with additional Zr. If grains of α-Fe further develop in the alloy, more resistance should be get over and more activation energy of crystallization should be required.

4 CONCLUSIONS

1) As heated to 900 ℃, the amorphous $Pr_8Fe_{86}B_6$ alloy consists of α-Fe phase, $Pr_2Fe_{23}B_3$ and $Pr_2Fe_{14}B$, whose average activation energies of crystallization are 214.88, 442.28 and 661.14 kJ/mol, respectively. At the beginning stage of crystallization, the activation energies of the three phases are about 306.09, 210.85 and 725.97 kJ/mol, respectively. During the crystallization process, the activation energy of α-Fe phase changes less as crystallized fraction is below 8%, and then reduces with increasing crystallized fraction. But the activation energies of $Pr_2Fe_{23}B_3$ and $Pr_2Fe_{14}B$ straightly decline with increasing crystallized fraction. While at the beginning stage of crystallization, the activation energies of the α-Fe phase in $Pr_8Fe_{85}Zr_1B_6$ and $Pr_8Fe_{84}Zr_2B_6$ alloys are 201.18 and 212.68 kJ/mol, respectively. Then the corresponding maximum, 347.18 and 432.04 kJ/mol, are obtained at φ= 10% of the crystallization fraction.

2) The reason for a coarse grain size obtained in annealing $Pr_8Fe_{86}B_6$ alloy is the behavior of difficult formation and easy growth. Additional Zr can change the crystallization behavior of the α-Fe phase in the amorphous Pr-Fe-B alloys, and metastable $Pr_2Fe_{23}B_3$ disappear during crystallization, which is helpful to the formation of the α-Fe/$Pr_2Fe_{14}B$ nanocomposite microstructure with a fine grain size for the α-Fe phase in the alloy.

[REFERENCES]

[1] Zhang X Y, Zhang J W, Wang W K. Crystallization process of an amorphous $Sm_8Fe_{85}Si_2C_5$ alloy under high pressure [J]. J Magn Magn Maer, 2001, 219: 199-205.

[2] Kuma J, Kitajima N, Kanai Y, et al. Maximum energy product of isotropic Nd-Fe-Fe-based nanocomposite magnets [J]. J Appl Phys, 1998, 83: 6623-6627.

[3] Schrefl T, Fidler H. Micromagnetic simulation of magnetizability of nanocomposite Nd-Fe-B magnets [J]. J Appl Phys, 1998, 83: 6262-6265.

[4] Fischer R, Kromüler. Importance of ideal grain boundaries of high remnant composite permanent magnets [J]. J Appl Phys, 1998, 83: 3271-3277.

[5] Schrefl T, Fidler J. Modelling of exchange-spring permanent magnets [J]. J Magn Magn Mater, 1998, 177-181: 970-974.

[6] Chang W C, Chiou D Y, Wu S H. High performance α-Fe/$Nd_2Fe_{14}B$-type nanocomposites [J]. Appl Phys Lett, 1998, 72: 121-123.

[7] Cormick P G Mc, Miao W F, Smith D A I, et al. Mechanically alloyed nanocomposite magnets (invited) [J]. J Appl Phys, 1998, 83: 6256-6261.

[8] Cheng Z H, Kronmüller, Shen B G. Magnetic properties of $Nd_8Fe_{77}Co_5B_6CuNd_3$ melt-spun ribbons [J]. Appl Phys Lett, 1998, 73: 1586-1589.

[9] Wang Z C, Zhou S Z, Qiao Y, et al. Effects of quenching rate on the phase transformation and magnetic properties of melt-spun $Pr_8Fe_{86}B_6$ ribbons during annealing [J]. J Magn Magn Mater, 2000, 218: 72-76.

[10] Wang Z C, Zhang M C, Zhou S Z, et al. Beneficial effects of Cu substitution on the microstructures and magnetic properties of Pr(FeCo)B/α-(FeCo) nanocomposites [J]. Journal of Alloys and Compounds, 2000, 309: 212-218.

[11] Zhang X Y, Zhang J W, Wang W K. Microstructure and magnetic properties of $Sm_2(Fe, Si)_{17}C_x$/α-Fe nanocomposite magnets prepared under high pressure [J], Appl Phys Lett, 1999, 74: 597-599.

[12] Zhang X Y, Zhang J W, Wang W K. A novel route for preparation of nanocomposite magnets [J]. Advanced Materials, 2000, 19: 1441-1444.

[13] Zhao T, Xiao Q F, Zhang Z D, et al. Effect of magnetocrystalline anisotropy on the magnetic properties of Fe-rich R-Fe-B nanocomposite magnets [J]. Appl Phys Lett, 1999, 75: 2298-2301.

[14] Zhang J W, Zhang X Y, Xiao F R, et al. Influence of pressures on the crystallization process of an amorphous $Fe_{73.5}Cu_1Nb_3Si_{13.5}B_9$ alloy [J]. Materials Letters, 1998, 36: 223-228.

[15] Zhang X Y, Zhang K Q, Liu J H, et al. Crystallization kinetics of amorphous $Sm_2(Fe, Si)_{17}C_x$/α-Fe alloy [J]. J Appl Phys, 2001, 89: 496-499.

[16] Gao L W, Shui Z T, Lu K, et al. Crystallization kinetics of amorphous Pb-Cu-Si alloys [J]. Acta Metallurgica Sinica, 1992, 28: 303-307.

[17] Wang Z C, Zhang M C. Nanocomposite $Pr_2(FeZr)_{14}B$/α-Fe permanent magnetic alloys [J] Metallic Function Material, 1998, 5(2): 65-67.

[18] Ma L Q, Wang L M, Zhang T. Effect of Zr and Nb elements on glass forming ability of Fe-B alloy [J]. Acta Metallurgica Sinica, 1999, 35: 661-633.

(Edited by HUANG Jin-song)